VOL. 82, NO. 8 JOURNAL OF GEOPHYSICAL RESEARCH MARCH 10, 1977

A LUNAR DENSITY MODEL CONSISTENT WITH TOPOGRAPHIC, GRAVITATIONAL, LIBRATIONAL, AND SEISMIC DATA

Bruce G. Bills

Division of Geological and Planetary Sciences,
California Institute of Technology, Pasadena, California 91125

Alfred J. Ferrari

Jet Propulsion Laboratory, Pasadena, California 91103

Abstract. A series of models of the lunar interior are derived from topographic, gravitational, librational, and seismic data. The librational parameters and low-degree gravity harmonics result primarily from surface height variations and only secondarily from lateral density variations. The moon departs from isostasy, even for the low-degree harmonics, with a maximum superisostatic stress of 200 bars under the major mascon basins. The mean crustal thicknesses under different physiographic regions are: mascons, 30-35 km; irregular maria, 50-60 km; and highlands, 90-110 km. A possible composition consistent with our model is an anorthositic crust, underlain by a predominantly forsterite upper mantle which grades into a refractory rich lower mantle surrounding a pyrrhotite core.

Introduction

Lunar interior models of increasing complexity are derived from topographic, gravitational, librational, and seismic data. A series of models, rather than only the final one, is presented in an effort to demonstrate the unique contribution of each data type and its effect on determining model parameters for the lunar density structure.

The various data types and their errors are discussed, and these data are cast into a form most convenient for internal model determination. The basic theory for this analysis is developed, and a series of lunar interior models are derived from the different data. Discussions are presented at each level of modeling, showing which data are satisfied and presenting the geophysical significance of that stage of the model development. Ultimately, a six-layered model is determined which satisfies all the data. The innovative aspects of this investigation are discussed in light of previous work, and the compositional implications of this lunar interior model are analyzed.

Basic Data

The topographic and gravitational data used consist of spherical harmonic coefficients of the surface shape and gravitational potential of the moon through degree and order 12 [Bills and Ferrari, 1976; Ferrari, 1975]. The topography and gravitational potential as functions of latitude θ and longitude ϕ are represented as

$$R(\theta, \phi) = R_0 \sum_{n=0}^{12} \sum_{m=0}^{n} T_{nm} \Lambda_{nm}(\theta, \phi)$$

$$\Phi(r, \theta, \phi) = \frac{GM}{R_0} \sum_{n=0}^{12} \left(\frac{R_0}{r}\right)^{n+1} \sum_{m=0}^{n} G_{nm} \Lambda_{nm}(\theta, \phi) \quad (1)$$

where T_{nm} and G_{nm} are topography and gravity harmonic coefficients, respectively, defined as

$$T_{nm} = [C_{nm}^{t}, S_{nm}^{t}] \quad , G_{nm} = [C_{nm}^{g}, S_{nm}^{g}]$$

and

$$\Lambda_{nm}(\theta, \phi) = P_{nm}[\sin(\theta)] \begin{bmatrix} \cos(m\phi) \\ \sin(m\phi) \end{bmatrix}$$

where P_{nm} are unnormalized associated Legendre functions of degree n and order m. G, M, and R_0 are the universal gravitational constant, the mass, and the mean radius, respectively, of the moon.

The physical librations of the moon are dependent upon both the low-degree gravity harmonics and the parameters (α, β, γ), which are defined in terms of the principal inertial moments $A < B < C$ as

$$\alpha = \frac{C - B}{A} \qquad \beta = \frac{C - A}{B} \qquad \gamma = \frac{B - A}{C} \quad (2)$$

Sinclair et al. [1976] have estimated the low-degree gravity harmonics and librational parameters from a combination of Doppler and laser-ranging data. Table 1 presents these estimates, the low-degree topography harmonics [Bills and Ferrari, 1976], and an estimate of the gravitational constant G [Heyl and Chrzanowski, 1942].

The resulting estimates for the lunar mean density and moments are

Copyright 1977 by the American Geophysical Union.

Paper number 6B0791.

TABLE 1. Lunar Gravitational, Topographic, and Librational Data

		Topography		Gravity	
n	m	$C_{nm}^{t} \times 10^6$	$S_{nm}^{t} \times 10^6$	$C_{nm}^{g} \times 10^6$	$S_{nm}^{g} \times 10^6$
0	0	10^6	...	10^6	...
1	0	-367.7 ± 44.6	...	...	...
1	1	-1049.3 ± 30.3	-255.4 ± 23.6	...	...
2	0	-303.9 ± 49.5	...	-203.62 ± 1.09	...
2	1	-193.4 ± 34.2	30.4 ± 24.9	...	...
2	2	7.4 ± 7.4	107.8 ± 9.4	22.40 ± 0.12	...

Three dots represent values that are zero by definition.
$G = (667.32 \pm 0.31) \times 10^{-10}$ cm^3 s^{-2} g^{-1}, $GM = (4902.796 \pm 0.003) \times 10^{15}$ cm^3 s^{-2}, $R_0 = (1737.59 \pm 0.24) \times 10^5$ cm, $\beta = (631.68 \pm 0.13) \times 10^{-6}$, and $\gamma = (227.82 \pm 0.08) \times 10^{-6}$.

$$\begin{aligned} \bar{\rho} &= 3.3437 \pm 0.0016 \text{ g cm}^{-3} \\ C &= (4C_{22}^{g}/\gamma)MR_0^2 = (0.3933 \pm 0.0021)MR_0^2 \\ I &= \frac{A+B+C}{3} = \left[\frac{3+\beta+\gamma-\beta\gamma}{3(1+\beta)}\right]C \\ &= (0.3931 \pm 0.0021)MR_0^2 \end{aligned} \tag{3}$$

In terms of moments M_n of the radial density distribution,

$$M_n \equiv (n+1)\int_0^1 \rho(\xi)\xi^n \, d\xi \tag{4}$$

where $\xi = r/R_0$. On the basis of the values listed in (3) the second and fourth moments are

$$\begin{aligned} M_2 &= \bar{\rho} = 3.3437 \pm 0.0016 \\ M_4 &= 5\bar{\rho}I/2MR_0^2 = 3.286 \pm 0.018 \end{aligned} \tag{5}$$

This form will prove useful for comparison with models to be derived later.

The seismic data used consist of (1) the inferred crustal structure in the region of the Apollo seismic array including discontinuities at depths of ~20 and 50-60 km [Toksöz et al., 1974] and (2) the travel time as a function of epicentral distance for P and S waves [Nakamura et al., 1974].

Theory

We will be mainly concerned with models consisting of nearly concentric nearly spherical shells of uniform density material. Each shell ℓ will be characterized by the normalized radius of its outer surface, $\xi_\ell = R_\ell/R_0$; a density contrast from the immediately overlying layer, $\Delta\rho_\ell = \rho_\ell - \rho_{\ell-1}$; and a set of spherical harmonic coefficients T_{nm}^{ℓ} which represent the shape of the outer surface of the layer. Thus the interface has the form

$$R(\theta, \phi) = R_0\xi_\ell \sum_{n=0}^{12}\sum_{m=0}^{n} T_{nm}^{\ell}\Lambda_{nm}(\theta, \phi) \tag{6}$$

The mean density and mean inertial moment of such a model are expressed by

$$M_2 = \bar{\rho} = \sum_\ell \Delta\rho_\ell \xi_\ell^3 \qquad M_4 = \frac{5\bar{\rho}I}{2MR_0^2} = \sum_\ell \Delta\rho_\ell \xi_\ell^5 \tag{7}$$

The complete inertia tensor of such a configuration is given by

$$I_{ij} = \frac{8\pi R_0^5}{15}\sum_\ell \Delta\rho_\ell (\xi_\ell)^5 L_{ij}^{\ell} \tag{8}$$

where

$$L_{11}^{\ell} = 1 + \frac{5}{2}\left[(S_{11}^{\ell})^2 + (C_{10}^{\ell})^2\right] + \frac{C_{20}^{\ell}}{2} - 3C_{22}^{\ell}$$

$$L_{22}^{\ell} = 1 + \frac{5}{2}\left[(C_{11}^{\ell})^2 + (C_{10}^{\ell})^2\right] + \frac{C_{20}^{\ell}}{2} + 3C_{22}^{\ell}$$

$$L_{33}^{\ell} = 1 + \frac{5}{2}\left[(C_{11}^{\ell})^2 + (S_{11}^{\ell})^2\right] - C_{20}^{\ell}$$

$$L_{12}^{\ell} = L_{21}^{\ell} = -\frac{5}{2}(C_{11}^{\ell}S_{11}^{\ell}) - 3S_{22}^{\ell}$$

$$L_{13}^{\ell} = L_{31}^{\ell} = -\frac{5}{2}(C_{11}^{\ell}C_{10}^{\ell}) - \frac{3}{2}C_{21}^{\ell}$$

$$L_{23}^{\ell} = L_{32}^{\ell} = -\frac{5}{2}(S_{11}^{\ell}C_{10}^{\ell}) - \frac{3}{2}S_{21}^{\ell}$$

The gravitational harmonics of the configuration are given by

$$\left(\frac{2n+1}{3}\right)\bar{\rho}G_{nm}^{\ell} = \sum_{\ell}\Delta\rho_{\ell}\xi_{\ell}^{n+3}T_{nm}^{\ell} \qquad (9)$$

to first order in the T_{nm}^{ℓ}. From the relation between the inertia tensor and the gravity harmonics

$$\begin{aligned} C_{20}{}^{g}M R_0^2 &= (I_{11} + I_{22} - 2I_{33})/2 \\ C_{21}{}^{g}M R_0^2 &= I_{13} = I_{31} \\ S_{21}{}^{g}M R_0^2 &= I_{23} = I_{32} \\ C_{22}{}^{g}M R_0^2 &= (I_{22} - I_{11})/4 \\ S_{22}{}^{g}M R_0^2 &= I_{12}/2 = I_{21}/2 \end{aligned} \qquad (10)$$

we note that for $n = 2$, (9) is merely the linear approximation to (8). We will thus use (8) in place of (9) for $n = 2$.

We will also be interested in the extent to which our models depart from isostatic equilibrium. This will be measured in terms of the variations about the mean of the hydrostatic pressure at the crust-mantle interface. The mean pressure at this level is approximately,

$$\bar{P} = (4\pi G R_0^2/3)\rho_0\bar{\rho}(1 - \xi_1) \qquad (11)$$

and the pressure deviations are

$$\Delta P(\theta, \phi) = \frac{4\pi G R_0^2}{3}\rho_0\bar{\rho}\sum_{n=1}^{12}\sum_{m=0}^{n}H_{nm}\Lambda_{nm}(\theta, \phi) \qquad (12)$$

where

$$H_{nm} = T_{nm}^{0} + (\Delta\rho_1/\rho_0)(\bar{\rho}_1/\bar{\rho})\xi_1^2 T_{nm}^{1}$$

and $\bar{\rho}_1$ is the mean density of the moon beneath the crust.

The rms isostatic pressure deviation as a function of harmonic degree is obtained from the normalized harmonics $\bar{H}_{nm} = H_{nm}/N_{nm}$, where the normalization factor is

$$N_{nm} = \left[(2n + 1)(2 - \sigma_{m0})\frac{(n - m)!}{(n + m)!}\right]^{1/2}$$

by

$$\sigma_n = \frac{4\pi G R_0^2}{3}\rho_0\bar{\rho}\left[\sum_{m=0}^{n}\bar{H}_{nm}^2\right]^{1/2} \qquad (13)$$

This will be useful in assessing the departure from isostasy as a function of wavelength.

In order to use seismic data as a constraint on lunar internal structure we will need to specify compressional and shear wave velocities V_p and V_s at each layer. These two velocities are determined by

$$V_p^2 = (K + 4\mu/3)/\rho \qquad V_s^2 = \mu/\rho \qquad (14)$$

where

$$K \equiv \rho(\partial P/\partial\rho)_S$$

is the adiabatic bulk modulus and μ is the shear modulus or rigidity. These in turn are functions of temperature and pressure for any given material. We will assume a linear dependence on temperature and pressure:

$$\begin{aligned} \rho(T, P) &= \rho_{STP} + (\partial\rho/\partial T)\Delta T + (\partial\rho/\partial P)\Delta P \\ K(T, P) &= K_{STP} + (\partial K/\partial T)\Delta T + (\partial K/\partial P)\Delta P \\ \mu(T, P) &= \mu_{STP} + (\partial\mu/\partial T)\Delta T + (\partial\mu/\partial P)\Delta P \end{aligned} \qquad (15)$$

A number of estimates of the lunar internal temperature distribution are available [e.g., Toksöz and Solomon, 1973]. All such models are characterized by a steep gradient near the surface and a more gradual gradient at depth. We will assume a temperature profile of the form [Nakamura and Latham, 1969]

$$T(\xi) = T(0) + \Delta T\xi^n \qquad (16)$$

with the parameters chosen to match the near-surface gradient and deep interior temperatures. A more complex model is not justified in light of the lack of constraints on the problem.

The pressure at each level is obtained by numerically integrating the equation of hydrostatic equilibrium. The pressure and temperature are then used to estimate the ambient density and elastic moduli from their assumed STP values.

The seismic travel times T and epicentral angles Δ are calculated from the velocity profile $V(\xi)$ for a given ray path by [Bullen, 1963]

$$T = 2R_0 \int_{\xi_m}^{1} \left[\eta^2 - \eta_m^2\right]^{-1/2} \frac{\eta^2 \, d\xi}{\xi}$$

$$\Delta = 2\eta_m \int_{\xi_m}^{1} \left[\eta^2 - \eta_m^2\right]^{-1/2} \frac{d\xi}{\xi} \qquad (17)$$

where $\eta = \xi/V(\xi)$ and η_m is the value of η at the midpoint of the ray path, where it reaches its minimum radius ξ_m.

Models

The simplest model considered has a uniform density of $\bar{\rho} = 3.3437$ g cm^{-3} and the outer surface is characterized by the topography harmonics T_{nm}^0. An interesting aspect of this model is that its liberational parameters are

$$\beta = (5.28 + 485.39) \times 10^{-6} = 490.67 \times 10^{-6}$$

$$\gamma = (5.65 + 45.29) \times 10^{-6} = 50.94 \times 10^{-6}$$

where the parenthetical terms are the first- and second-degree contributions, respectively. We thus conclude that the first-degree harmonics are of little consequence dynamically in comparison to the second-degree harmonics. Comparing these estimates with the values in Table 1, we note that the assumption of uniform density, coupled with the actual topography, gives, at least qualitatively, reasonable estimates of β and γ, whereas Kopal [1969] has shown that the rotational and tidal distortions of a hydrostatic moon would yield

$$\beta = 37.39 \times 10^{-6} \qquad \gamma = 27.97 \times 10^{-6}$$

Two basic conclusions are obtained from this comparison: first, the orientation and rotational dynamics of the moon are intrinsically determined primarily by surface height variations and only secondarily by lateral density variations, and second, the moon is not well approximated by a hydrostatic model [Kopal, 1969].

We now turn our attention to models with a radial density variation. The simplest such model considered consists of two concentric spherical shells having a density ρ_0 in the outer shell and a density contrast $\Delta\rho_1$ across the interface at a normalized radius of $R_1/R_0 = \xi_1$. A weak compositional constraint is assumed in that

$$2.7 \le \rho(\xi) \le 5.4 \text{ g cm}^{-3}$$

where the lower bound corresponds roughly to anorthosite and the upper bound to an Fe-FeS eutectic composition [Brett, 1973] at the lunar central pressure (~50 kbar) and room temperature. These bounds are shown by the dot-dash lines in Figure 1. If in addition, the model is constrained to have the observed mean density and density inversions with depth are not allowed, the envelope of acceptable density profiles is given by the dashed lines in Figure 1. When the model is subjected to the additional constraint that it have the correct mean moment of inertia, the resulting density bounds are those given by the solid lines in Figure 1.

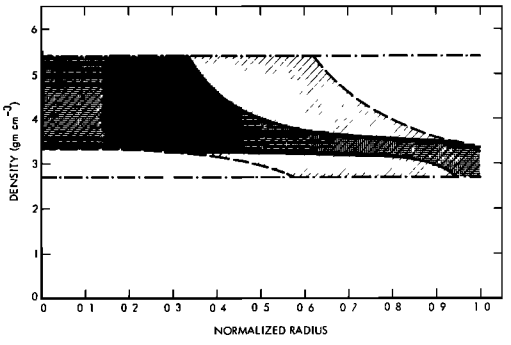

Fig. 1. Envelope of plausible density profiles.

These lower and upper bounds for the mean moment of inertia are simply the solutions for $\rho_0(\xi)$ and $\rho_0(\xi) + \Delta\rho_1(\xi)$, respectively, subject to

$$2.7 \le \rho_0 \le \rho_0 + \Delta\rho_1 \le 5.4$$

$$\rho_0 + \Delta\rho_1 \xi_1^3 = M_2 = 3.3437 \qquad \rho_0 + \Delta\rho_1 \xi_1^5 = M_4 = 3.286$$

They represent the envelope of all possible monotonic density distributions subject to the above constraints. However, not all models falling within these bounds are allowed. In particular, a uniform density model is inconsistent with these constraints. Although these bounds are not tight enough to be of real value in determining the composition of the lunar interior, they do exclude such extreme cases as either a uniform density or an Fe-Ni core with a radius of 380 km or greater. These bounds are also useful in conjunction with other data types.

The next step in complexity is to allow the model to depart from spherical symmetry in order to match not only the actual topography, as was done before, but also the gravitational potential to degree and order 12 and the entire inertia tensor, three moments and three products of inertia, rather than just the mean moment. To do this, we start by including the first- and second-degree harmonics T_{nm}^{ℓ} (ℓ = 0, 1; n = 1, 2) describing the shape of the outer surface and the crust-mantle interface. The eight harmonics T_{nm}^0 (three first degree and five second degree) of the outer layer are known from the observed topography [Bills and Ferrari, 1976] (see Table 1), but the crustal density ρ_0 and the eight harmonics of the crust-mantle interface T_{nm}^1, as well as the density contrast $\Delta\rho_1$ and the normalized radius $\xi_1 = R_1/R_0$, are unknown and must be determined from (8) and (9) by constraining the inertia tensor of the model to the observed values. Equation (9) applied to the first-degree harmonics ensures that the center of figure of the mantle is offset in such a way as to counterbalance the center of figure

TABLE 2. Two-Layered Lunar Density Model Representative Solutions

Parameter	A Priori	A Posteriori for $R_c = 0$	A Posteriori for R_c = 400 km and ρ_c = 5.4 g cm^{-3}
ρ_0, g cm^{-3}	2.90 ± 0.20	2.72 ± 0.07	2.75 ± 0.06
$\Delta\rho$, g cm^{-3}	0.50 ± 0.20	0.74 ± 0.08	0.64 ± 0.07
T_c, km	69.5 ± 17.4	95.7 ± 15.6	73.2 ± 15.8
ΔX_1, km	0.00 ± 1.64	8.33 ± 1.20	9.40 ± 1.30
ΔX_2, km	0.00 ± 1.64	2.53 ± 0.56	2.86 ± 0.40
ΔX_3, km	0.00 ± 1.64	1.40 ± 0.20	1.57 ± 0.22
C_{20}^1, 10^{-4}	0.00 ± 10.00	-7.98 ± 0.63	-8.40 ± 0.66
C_{21}^1, 10^{-4}	0.00 ± 10.00	10.45 ± 1.51	11.43 ± 1.59
S_{21}^1, 10^{-4}	0.00 ± 10.00	-0.25 ± 0.04	-0.27 ± 0.04
C_{22}^1, 10^{-4}	0.00 ± 10.00	0.45 ± 0.004	0.44 ± 0.01
S_{22}^1, 10^{-4}	0.00 ± 10.00	-5.71 ± 0.84	-6.26 ± 0.89

displacement of the outer layer.

Such a model has 11 unknown parameters (T_{nm}^1 (eight), ρ_0, $\Delta\rho_1$, and ξ_1) but only 10 constraints (G_{lm} (three), I_{ij} (six), and $\bar{\rho}$). However, we have some a priori knowledge about each of the parameters, and since this makes the system effectively overdetermined, we can perform a weighted least squares inversion. See Table 2 for some representative results. Therein are presented the a priori and a posteriori estimates and uncertainties for each of the 11 parameters for both the nominal solution and a solution with a core of radius R_c = 400 km and density ρ_c = 5.4 g cm^{-3}. The first-degree harmonics are presented in terms of the corresponding center of figure displacement

$$\Delta X = R_0\xi_1(C_{11}^1, S_{11}^1, C_{10}^1)$$

and the crustal thickness is $T_c = R_0(1 - \xi_1)$.

We discover two important facts from this model. First, in the case with no core the mean crustal thickness is significantly greater than that inferred from the locally derived seismic value, even though the densities are quite reasonable. This conflict can be removed by inclusion of a region of higher density at depth. Although the core model presented (R_c = 400 km and ρ_c = 5.4 g cm^{-3}) is by no means unique, the amount of density increase required is greater than can be accounted for by self-compression of a homogeneous moon for any reasonable elastic moduli and temperature profile.

Second, this model may be shown to depart from isostatic equilibrium, even for the low-degree harmonics. We shall have more to say about isostasy later.

Having established the inadequacy of a two-layered model, we will now present a more detailed model in which the density, elastic moduli, and temperature are all allowed to vary more or less continuously with depth. Our analyses have shown that a three-layered model satisfies the constraints imposed by the gravitational, topographic, and librational data. However, current seismic studies [e.g., Nakamura et al., 1974] suggest a more complex internal structure. The model that we have chosen has six distinct regions, and the approximate depths to the boundary interfaces are upper and lower crust, 20 and 70 km and upper, middle, and lower mantle, 300, 800, and 1400 km. The core has a radius of 340 km. The crustal and upper mantle interfaces correspond to seismic discontinuities [Toksöz et al., 1974; Nakamura et al., 1974]. The middle and lower mantle and core are inferred from deep seismic events [Nakamura et al., 1974], electrical conductivity profiles [Dyal et al., 1976], and thermal and compositional constraints [Brett, 1973]. For modeling purposes the normalized radii of the interfaces are taken to be ξ_ℓ = 1.00, 0.99, 0.96, 0.83, 0.54, and 0.20.

Within each region the STP density and elastic moduli are assumed to vary linearly with depth between the values specified at the upper and lower boundaries. The ambient density and elastic moduli at each layer are then calculated from the STP values and the ambient temperature and pressure.

The assumed temperature and pressure derivatives of the density and elastic moduli correspond in the crust to anorthosite [Baldridge and Simmons, 1971], in the mantle to forsterite, and in the core to pyrite [Skinner, 1966; Birch, 1966]. The STP density and bulk modulus of the core are those estimated for an Fe-FeS eutectic composition [Brett, 1973; Brett and Bell, 1969; King and Ahrens, 1973]. The crustal density profile is from Gast and Giuli [1972], and the elastic moduli were chosen to duplicate a suitable average of the crustal velocity profile as given by Toksöz et al, [1974].

The lunar temperature profile is imprecisely known, particularly in the deep interior [e.g., Toksöz and Solomon, 1973]. We have assumed surface and central temperatures of 250° and 1900°K, respectively, and have treated the actual temperature distribution with depth as a variable deter-

TABLE 3a. Lunar Interior Structure Model

ξ	Depth, km	Temperature, °K	Pressure, kbar	ρ, g cm^{-3}	K, Mbar	σ	V_p, km s^{-1}	V_s, km s^{-1}
				Upper Crust				
1.00	0	250	0.00	2.703	0.410	0.250	5.22	3.02
0.99	20	315	0.76	2.703	0.410	0.250	5.22	3.02
				Lower Crust				
0.99	20	315	0.76	2.852	0.651	0.293	6.12	3.31
0.96	70	499	3.19	2.950	0.769	0.296	6.52	3.51
				Upper Mantle				
0.96	70	499	3.19	3.371*	1.222*	0.246*	8.11	4.71
0.83	300	1117	14.57	3.382*	1.234*	0.275*	7.89	4.39
				Middle Mantle				
0.83	300	1117	14.57	3.408*	1.234*	0.275*	7.89	4.39
0.54	800	1760	34.36	3.397*	1.691*	0.420*	7.80	2.89
				Lower Mantle				
0.54	800	1760	34.36	3.399*	1.691*	0.420*	7.80	2.89
0.20	1400	1897	48.13	3.424*	1.745*	0.443*	7.68	2.46
				Core				
0.20	1400	1897	48.13	5.209	1.400	0.500	5.18	0.00
0.00	1740	1900	52.95	5.223	1.423	0.500	5.22	0.00

*Parameter which was varied in search for acceptable model.

mined by the parameter n in (16). The value ultimately used was n = 4.0.

A family of models is generated by varying the density and elastic moduli at the mantle region interfaces (ξ = 0.96, 0.83, 0.54, and 0.20) subject to the constraints that (1) the STP values of ρ, K, and Poisson's ratio σ = (3K − 2μ)/(6K + 2μ) are all nondecreasing with depth and (2) K and σ are continuous across the interfaces at ξ = 0.83 and 0.54. The STP values of ρ, K, and σ at intermediate points are found by linear interpolation, and the ambient values of these parameters are found, as they were before, from the ambient temperature and pressure. These perturbations are performed until a model is found which has the desired mean density and moment as well as P and S wave travel times. The resultant temperature, pressure, density, bulk modulus, Poisson ratio, and seismic velocity profiles of such a model are given in Table 3a. Table 3b gives the moments of the density distribution M_n (n = 0, 1, ..., 8). The seismic travel time as a function of epicentral distance for the model is compared with observed teleseismic data [Nakamura et al., 1974] in Figure 2. The seismic phases shown are identified according to the nomenclature usually applied to the earth [Jeffreys, 1959].

We tentatively interpret the P wave arrivals near Δ = 150° as rays diffracted around the core and the weak arrival at Δ = 168° as a PKP_2 phase (not shown in the figure) due to a rapid decrease in seismic velocity at the mantle-core interface.

TABLE 3b. Moments of Density Distribution M_n

n	M_n	n	M_n	n	M_n
0	3.7409	3	3.3101	6	3.2496
1	3.4247	4	3.2875	7	3.2322
2	3.3433	5	3.2679	8	3.2156

Observed values are M_2 = 3.3437 ± 0.0016 and M_4 = 3.2858 ± 0.0211.

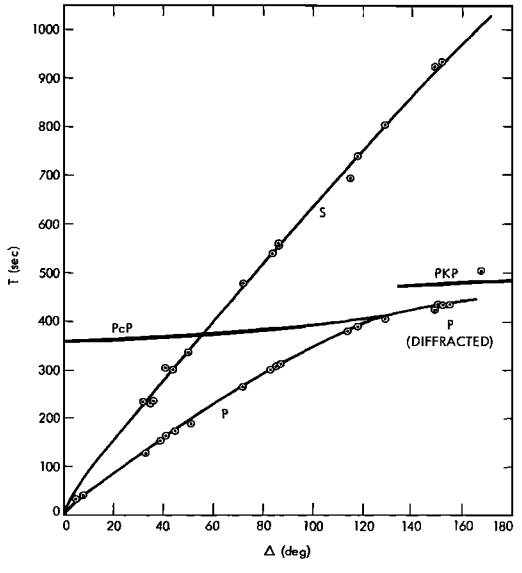

Fig. 2. Lunar seismic travel times. Curves represent model calculations; circles with dots represent data [Nakamura et al., 1974].

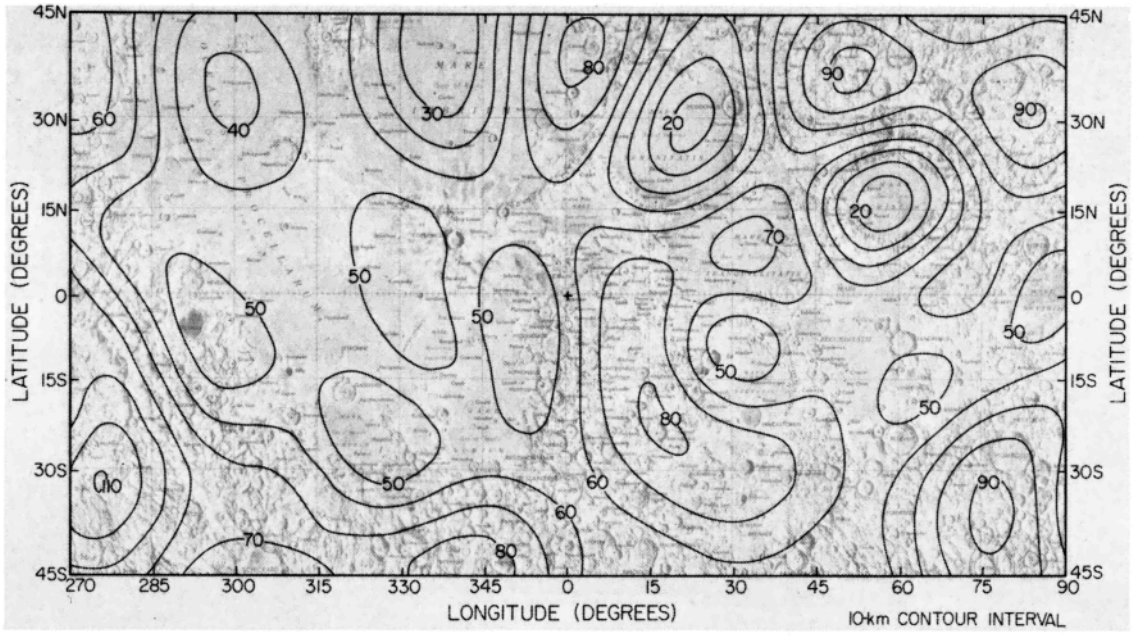

Fig. 3a. Crustal thickness variations on the lunar near side.

A comparison of the STP density and elastic moduli with those of olivine and pyroxene [Chung, 1970; Nakamura et al., 1974] reveals that a mineral assemblage consisting largely of olivine (80-85% forsterite) and some pyroxene is consistent with the upper mantle model. The increase in density and bulk modulus with depth is consistent with an increase in CaO, TiO_2, and/or Al_2O_3 [Simmons and Wang, 1971; Anderson, 1975].

Given values for the mean crustal thickness and density and the density contrast with the mantle, we can include the higher harmonics of topography and gravity in our model, solving for T_{nm}^1 from T_{nm}^0 and G_{nm} by (8) and (9). We are thus able to estimate the variation of crustal thickness over the planet on the assumption that all lateral density variations occur as undulations on the mantle-crust interface, which is at a depth of 50-60 km in the area of the Apollo seismic array. For the densities in our model a mean crustal thickness of 70 km is required to match the seismic values. The resultant crustal thickness map is presented in Figures 3a and 3b. Wood [1973] has presented a similar analysis based on a more restricted data set. He inferred crustal thicknesses which are systematically less than our estimates.

The crustal thickness indicated in the mascon basins is somewhat of an underestimate, since the effect of a surface layer of basalt is ignored. Bowin et al. [1975] estimate that such a surface fill accounts for roughly 20% of the observed

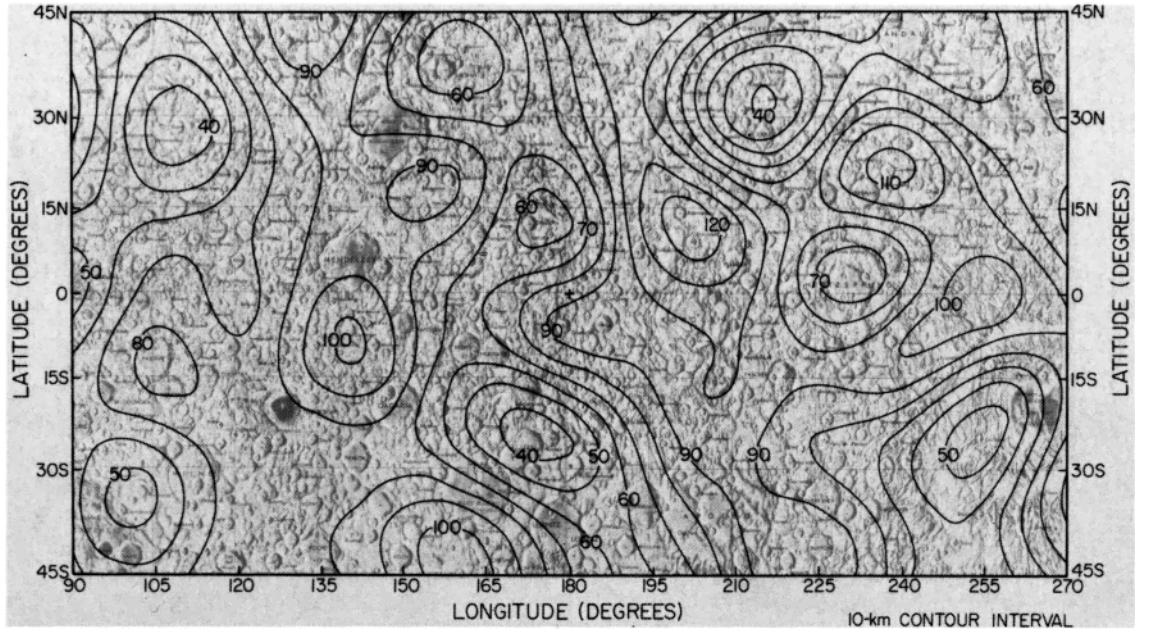

Fig. 3b. Crustal thickness variations on the lunar far side.

TABLE 4. Root-Mean-Square Nonisostatic Stresses Versus Harmonic Degree

Degree n	Stress σ_n, bars	Half Wavelength $L_n = \pi R_0/n$, km
1	5.42	5460
2	16.86	2730
3	6.67	1820
4	8.70	1365
5	14.92	1092
6	26.03	910
7	27.50	780
8	17.52	683
9	17.09	607
10	13.61	546
11	31.94	496
12	15.15	455

gravity anomaly. They estimate a mantle uplift in Mare Serenitatis of 12 km, compared to our estimate of roughly 50 km. However, there is a factor of 2 discrepancy between the free-air anomaly estimates used, and the fact that Bowin et al. are modeling only free-air gravity, whereas we are modeling Bouguer gravity, accounts for an additional factor of 2.

The mean crustal thicknesses under different physiographic regions are mascons, 30-35 km; irregular maria, 50-60 km; and highlands, 90-110 km.

As was previously mentioned, this model is not in isostatic equilibrium; i.e., the pressure at the crust-mantle interface varies with position about its mean value of 3.2 kbar. The maximum superisostatic stress, as calculated from (12), is the value slightly in excess of 200 bars associated with the major mascon basins Imbrium, Serenitatis, and Crisium. Other regions have smaller stresses, and the global rms stress variation is 64 bars. The rms superisostatic pressure as a function of harmonic degree, from (13), is given in Table 4.

There are several significant aspects of this calculation. First, it is not true that the first-degree harmonics are isostatically compensated by definition as has been assumed [e.g., Phillips and Saunders, 1975]. The fact that the first-degree harmonics of the free-air gravity are zero by definition has no bearing on isostasy. There is a large contribution from harmonic degrees 5-9. The fact that these harmonics have half wavelengths comparable in size to the major mascons may be significant. However, the harmonic spectrum is affected by the spatial distribution of the anomalies as well as their size. Lastly, the large contribution from degree 11 is likely an artifact of the data distribution. The high-degree harmonics are not well determined.

It should be noted that it is possible to produce a model which satisfies both topographic and gravitational data and is also isostatically compensated at depth. However, when such models were attempted, the depth of compensation of the low-degree harmonics approached that of the presently proposed mantle-core interface. Since the superisostatic stresses implied by the above model are close to the stresses found in the earth, it appears more reasonable to accept a nonisostatic moon.

Summary

We have presented a series of lunar models culminating in a six-layered model with undulations on the outer surface and at the crust-mantle interface. This model is consistent with all available topographic, gravitational, librational, and seismic data.

We have concluded that the librational parameters of the moon are determined primarily by surface height variations and only secondarily by lateral density variations and that the surface topography is not isostatically supported, nor is it predominated by a fossil tidal or rotational bulge. The largest pressure departures from isostasy are approximately 200 bars under the major mascon basins. The crustal thickness varies from 30-35 km under mascon basins to 90-110 km under the highlands, with the irregular maria intermediate at 50-60 km.

All of the data considered are consistent with an anorthositic crust extending to a mean depth of 70 km underlain by a predominantly forsterite upper mantle grading into a refractory-rich lower mantle surrounding a pyrrhotite core. Such a composition is consistent with but not uniquely specified by our model calculations.

We note that a smaller estimate of the mean inertial moment would be consistent with a larger core, which in turn would simplify the interpretation of the P wave arrival times near $\Delta = 150$ and at 168 deg, which are presently interpreted as diffracted P and PKP_2, respectively.

Acknowledgments. We would like to express appreciation to R. J. Phillips for support and valuable discussions during this investigation. This report represents one phase of research performed at both the Jet Propulsion Laboratory and the California Institute of Technology under NASA contract NAS 7-100. Division of Geological and Planetary Sciences, California Institute of Technology, contribution 2751.

References

Anderson, D. L., On the composition of the lunar interior, J. Geophys. Res., 80, 1555-1557, 1975.

Baldridge, W. S., and G. Simmons, Thermal expansion of lunar rocks, Proc. Lunar Sci. Conf. 3rd, 2317-2321, 1971.

Bills, B. G., and A. J. Ferrari, A harmonic analysis of lunar topography, submitted to Icarus, 1976.

Birch, F., Compressibility; Elastic constants, Handbook of Physical Constants, Geol. Soc. Amer. Mem., Sect. 7, 97, 97-173, 1966.

Bowin, C., B. Simon, and W. R. Wollenhaupt, Mascons: A two-body solution, J. Geophys. Res. 80, 4947-4955, 1975.

Brett, R., A lunar core of Fe-Ni-S, Geochim. Cosmochim. Acta, 37, 165-170, 1973.

Brett, R., and P. M. Bell, Melting relations in the Fe-rich portion of the system Fe-FeS at 30 kb pressure, Earth Planet. Sci. Lett., 6, 479-482, 1969.

Bullen, K. E., An Introduction to the Theory of Seismology, pp. 109-113, Cambridge University Press, New York, 1963.

Chung, D. H., Effects of Fe/Mg ratio on V_p and V_s in olivine, J. Geophys. Res. 75, 7353-7361, 1970.

Dyal, P., C. W. Parkin, and W. D. Daily, Structure of the lunar interior from magnetic field measurements (abstract), in Lunar Science VII, pp. 224-226, Lunar Science Institute, Houston, Tex., 1976.

Ferrari, A. J., Lunar gravity: The first farside map, Science, 188, 1297-1300, 1975.

Gast, P. W., and R. T. Giuli, Density of the lunar interior, Earth Planet. Sci. Lett., 16, 299-305, 1972.

Heyl, P. R., and P. Chrzanowski, A new determination of the constant of gravitation, Radio Sci. 29, 1-31, 1942.

Jeffreys, H., The Earth, pp. 87-93, Cambridge University Press, New York, 1959.

King, D. A., and T. J. Ahrens, Shock compression of FeS, Nature London Phys. Sci., 243, 82-83, 1973.

Kopal, Z., The Moon, pp. 77-90, D. Reidel, Dordrecht, Netherlands, 1969.

Nakamura, Y., and G. V. Latham, Internal constitution of the moon, J. Geophys. Res., 74, 3771-3780, 1969.

Nakamura, Y., G. Latham, D. Lammlein, M. Ewing, F. Duennebier, and J. Dorman, Deep lunar interior inferred from recent seismic data, Geophys. Res. Lett., 1, 137-140, 1974.

Phillips, R. J., and R. S. Saunders, The isostatic state of Martian topography, J. Geophys. Res., 80, 2893-2898, 1975.

Simmons, G., and H. Wang, Single Crystal Elastic Constants and Calculated Aggregate Properties: A Handbook, 2nd ed., 370 pp., MIT Press, Cambridge, Mass., 1971.

Sinclair, W. S., W. L. Sjogren, J. G. Williams, and A. J. Ferrari, The lunar moment of inertia derived from combined Doppler and laser ranging data (abstract), in Lunar Science VII, p. 817, Lunar Science Institute, Houston, Tex., 1976.

Skinner, B. J., Thermal expansion, Handbook of Physical Constants, Geol. Soc. Amer. Mem., Sect. 6., 97, 75-96, 1966.

Toksöz, M. N., and S. C. Solomon, Thermal history and evolution of the moon, Moon, 7, 251-278, 1973.

Toksöz, M. N., A. M. Dainty, S. C. Solomon, and K. R. Anderson, Structure of the moon, Rev. Geophys. Space Phys., 12, 539-567, 1974.

Wood, J. A., Bombardment as a cause of the lunar asymmetry, Moon, 8, 73-103, 1973.

(Received May 5, 1976;
revised October 1, 1976;
accepted October 18, 1976.)